Cellular arrays during upward solidification of Pb-30 wt% T1 alloys

H. Nguyen Thi, B. Billia, L. Capella

Classification
Physics Abstracts
81.30F — 68.70 — 61.70 — 47.90

Cellular arrays during upward solidification of Pb-30 wt% Tl alloys

H. Nguyen Thi, B. Billia and L. Capella

Laboratoire de Physique Cristalline, Faculté de St Jérôme, Case 151, avenue Escadrille Normandie-Niemen, 13397 Marseille Cedex 13, France

(*Reçu le 3 mars 1989, révisé le 28 novembre 1989, accepté le 20 décembre 1989*)

Résumé. — Nous présentons une étude quantitative des réseaux hexagonaux, cellulaires ou dendritiques, obtenus lors de la solidification vers le haut d'alliages Pb-30 % en poids Tl. Ces réseaux sont reconstitués par la méthode de Wigner-Seitz, ce qui permet la détermination de l'espacement primaire, l'identification des défauts du réseau et l'analyse, à partir de concepts développés pour la fusion bidimensionnelle, de la désorganisation des structures interfaciales.

Abstract. — A quantitative study of the cellular or dendritic hexagonal arrays, obtained during upward solidification of Pb-30 wt% Tl alloys, is presented. These arrays are reconstituted by the Wigner-Seitz method which allows the determination of the primary spacing, the identification of the defects and the analysis of the disorganization of the interface structures by using concepts developed for two-dimensional melting.

Introduction.

Recent theoretical advances on the propagation of Saffman-Taylor fingers, growth of a free dendrite and cellular solidification [1-3], have given a new impetus to the analysis of structure selection in systems forming interfacial patterns. Concerning directional solidification of binary alloys, there is a need of precise experimental data especially in the cellular domain. The aim of the paper is to report observations on cellular (and dendritic) arrayed growth during upward solidification of Pb-30 wt% Tl alloys, with solutal-driven convection in the liquid phase. The emphasis is laid (i) on the influence of fluid flow on the primary spacing λ, which is determined from a reconstruction of the structure, and (ii) on the defects and disorder of the interfacial array.

The spatial structuration of the solid-liquid interface is controlled by the temperature gradient in the liquid G_L, the solute concentration C_∞ and the growth velocity V. For given

(*) U.A. au CNRS n° 797.

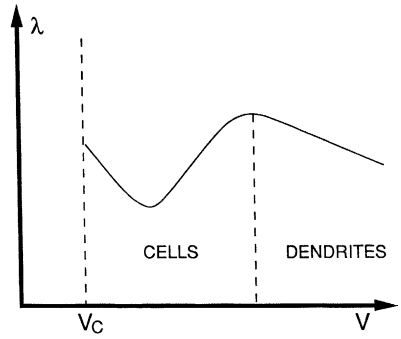

Fig. 1. — Schematic diagram showing the variation of the primary spacing λ with the growth velocity V, for cells and dendrites.

C_∞ and G_L, the interface morphology changes from planar to cellular to dendritic as V is increased. In the absence of convection in the melt, these morphological transitions are easily defined from the variation of the periodicity λ with V [4] as shown in figure 1. A cell or a dendrite can be characterized by shape parameters, e.g. λ. All experimental variables and the thermophysical properties of the alloy can be properly taken into account by means of three lengthscales : a solutal length

$$\ell_S = D/V \,, \tag{1}$$

a thermal length

$$\ell_t = mC_\infty(K-1)/KG_L \,, \tag{2}$$

and a capillary length

$$d_0 = \Gamma K/mC_\infty(K-1) \tag{3}$$

where D is the diffusion coefficient of the solute in the melt, m the liquidus slope, K the solute partition coefficient, and Γ the capillary coefficient. In a non-dimensional formulation [5, 6], the characteristics of the patterns ultimately depend on the level $\nu = \ell_t/\ell_S$ of morphological instability and on the absolute-stability parameter $A = Kd_0/\ell_S$, introduced by Mullins and Sekerka [7], which contains capillarity. A level $\nu > 1$ corresponds to the existence of constitutional supercooling in a liquid layer ahead of a flat solidification front [8].

The critical wavelength λ_S of morphological instability of a planar solidification front is given by the linear stability analysis [7] and is actually observed when the bifurcation is supercritical [9]. Under diffusion control, this is always the case for alloys whose segregation coefficient is greater than 0.45 [10, 11], among which lead-thallium alloys for which K is slightly higher than unity. Besides these calculations using amplitude expansions, computations [12] have been developed in order to predict the nonlinear structures close to the threshold.

All these analyses do not consider convection in the liquid phase which is quite common on the ground, in particular at low growth velocities. Concerning thermosolutal instability, a lot of work has, since the pioneering study of Coriell *et al.* [13], been dedicated to the understanding of the coupling between the convective and morphological branches [14, 15].

With β minus the coefficient of solutal expansion, g the acceleration of gravity, η the kinematic viscosity and

$$G_C = C_\infty (K-1)/K\ell_S \,, \tag{4}$$

solutal convection is characterized by the Rayleigh number

$$R_S = \beta g G_C \ell_S^4 / \eta D \tag{5}$$

and by the wavelength λ_{SC} at the onset.

The main result is that there is only a negligible interplay due to the large difference in the critical wavelengths λ_{SC} and λ_{MS} of respectively the pure hydrodynamic and morphological instabilities ($\lambda_{SC} \gg \lambda_{MS}$). It follows that, in practice, it is still possible to define a velocity threshold for morphological instability (of Mullins-Sekerka type) even when the experiments are performed in the presence of solutal convection in the melt. Indeed, while being modulated at the convective scale λ_{SC}, the solid-liquid interface remains *locally* planar at the scale λ_{MS}. The stabilizing effect of outer convection on the solutal instability was investigated by Hennenberg *et al.* in a boundary layer approach [16]. Sidewalls are taken into account by McFadden *et al.* [17] and by Guérin *et al.* [18]. It should be noticed that, in practical situations, solutal convection occurs in a medium which is highly confined from the side [19] whereas the phase boundary is laterally infinite for the morphological patterns.

2. Experiments.

2.1 EXPERIMENTAL PROCEDURE. — Lead-thallium alloys are solidified upwards in the Bridgman set up which was previously used [20]. The samples are grown in a boron nitride crucible of 0.95 cm inner diameter and 12.5 cm long. The thermal conductivity of boron nitride is close to that of the metallic alloy, which favors the flatness of the isotherms close to the wall.

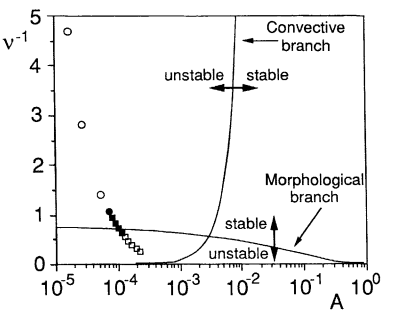

Fig. 2. — Diagram of solutal convection in the liquid phase superimposed on the basic diagram ν^{-1} *versus* A for morphological instability of a planar solidification front. Experimental points : (○) no microstructure ; (●) elongated cells ; (■) cells ; (□) dendrites.

Experiments are carried out for a thallium concentration $C_\infty = 30$ wt%, in a temperature gradient $G_L = 40$ °C/cm or thereabout, for growth velocities V ranging from 0.15 to 2 cm/h. These experiments are plotted on the classical diagram for morphological instability, which gives ν^{-1} *versus* A [21], upon which the domain of convective instability is superposed (Fig. 2). After some transformations of equation (5) with $R_S = R_{S,C}$, where $R_{S,C}$ is the critical

Rayleigh number for hydrodynamic instability, the onset ν_{SC} of solutal convection is rewritten

$$\nu_{SC}^{-1} = \frac{2\,mK_L\,G_L}{K^2(K_S + K_L)\,\Gamma^2} \frac{\eta D R_{S,C}}{\beta g} A^2 \tag{6}$$

where K_L and K_S are the thermal conductivities of liquid and solid. The theoretical limits are calculated for the values of the thermophysical properties of the Pb-Tl alloys given in table I. All the data points are in the region of solutal convection, which modulates the solid-liquid interface on the macroscopic scale of the crucible [19, 22], so that the study of the effect of fluid flow on the interfacial microstructure is meaningful. The convective level can be characterized by the ratio $R_S/R_{S,C}$. As $R_{S,C} = 12.4$ for $K = 1.1$ (see Tab. I in Ref. [15]), this ratio decreases from 3×10^5 to 130 with increasing velocity. This is due to the fact that the gradient G_C, the strength for instability which is proportional to ℓ_S^{-1}, acts on a width which is of the order of ℓ_S but enters to the 4th power into the definition of R_S.

Table I. — *Thermophysical properties of* Pb-30 wt% Tl *alloys.*

Segregation coefficient K	1.1
Liquidus slope m	1 K/wt%
Liquid thermal diffusivity	0.108 cm^2/s
Liquid kinematic viscosity η	2.43×10^{-3} cm^2/s
Thallium diffusivity in the melt D	2×10^{-5} cm^2/s
Solutal expansion coefficient of the liquid $-\beta$	-5.3×10^{-4} $wt\%^{-1}$
Capillary coefficient Γ	2×10^{-5} K.cm
Liquid thermal conductivity K_L	0.155 J/cm Ks
Solid thermal conductivity K_S	0.314 J/cm Ks

When half solidified, each Pb-Tl sample is quenched to retain the shape of the solid-liquid interface whose determination, both on the macroscopic level, in order to catch the effect of solutal rolls [19] and on the scale of the morphological pattern, is not a straightforward task. We have thus developed a method of repeated polishings followed by chemical etchings on a thick slice which contains the solid-liquid region. Within this zone, the microsegregation of thallium is high enough for the etching to be very sensitive so that we are able to get closely-spaced micrographs. With this procedure, the macroscopic shape of the solidification front is deduced from the contour lines seen at each step and a precise knowledge of the cellular (or dendritic) array is obtained from the microstructure which is revealed place after place on completing the process.

The primary spacing λ is determined and defects are analyzed by the Wigner-Seitz method, which for instance has been otherwise used to study disorder in Bénard-Marangoni

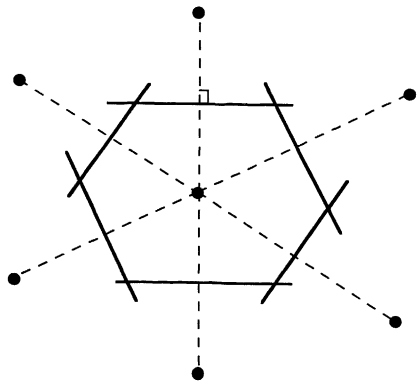

Fig. 3. — Wigner-Seitz reconstruction of a cell. Full circles correspond to cell centers.

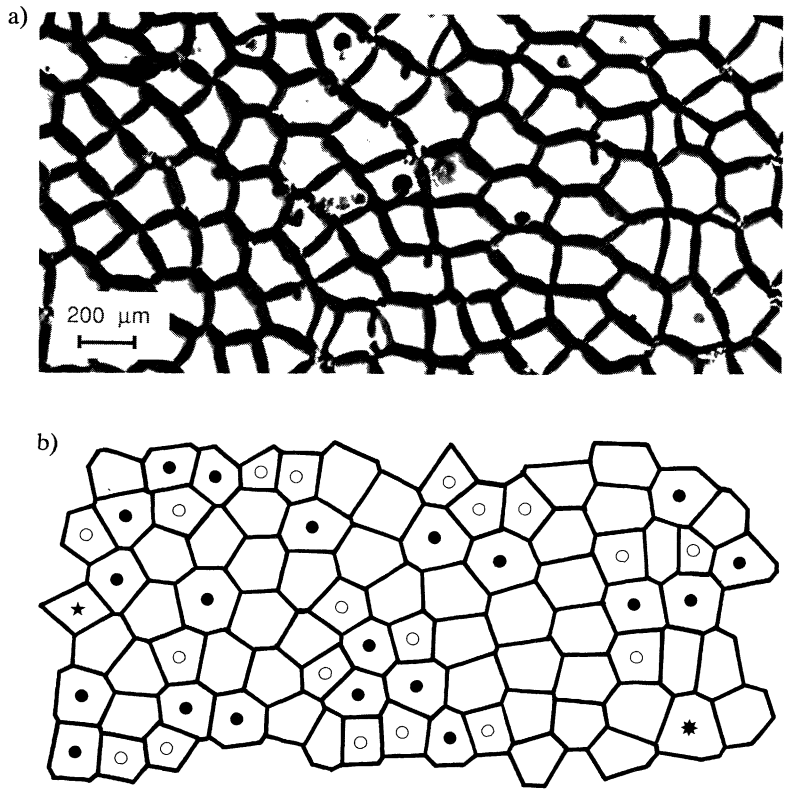

Fig. 4. — $V = 1.10$ cm/h. a) Cellular array (chemical etching on a transverse section). b) Array reconstruction (⋆) square (○) pentagon (●) heptagon (✱) octagon.

convection and nematic-shear flow instabilities [23]. First, black-and-white prints at high enough magnification are taken from the negatives, i.e. with a cellular spacing about 1 cm. On these prints, the positions of the cell centers are digitized by manual plotting on a HP 9114 graphic tablet, the accuracy of which is ± 0.6 mm. The nearest neighbours of each cell are then identified without ambiguity through a Wigner-Seitz reconstruction for which one draws

the segments joining the cell center to its neighbours within 2 to 3 times the presumed periodicity. Next, the segment mid-perpendiculars are drawn. The « reconstructed » cell is finally taken as the smallest polygon which can be defined by these mid-perpendiculars (Fig. 3). The 2D-cellular array is thus reconstituted cell by cell (Fig. 4) which allows the subsequent study of the defects.

A code evaluates all the intercellular distances (distances from a cell center to the centers of the first neighbours) whose average over about 300 cells is taken as the center-to-center distance r. The cells form an imperfect honeycomb which will be characterized by the primary spacing $\lambda = r\sqrt{3}/2$, the percentage of defects d_S and correlation functions.

2.2 MICROSTRUCTURAL TRANSITIONS. — For the three lower growth velocities ($V = 0.15$, 0.25 and 0.5 cm/h) no trace of morphological instability (no microstructure at the scale λ_{MS}) has been evidenced in any place on the undulated solidification front (open circles in Fig. 2).

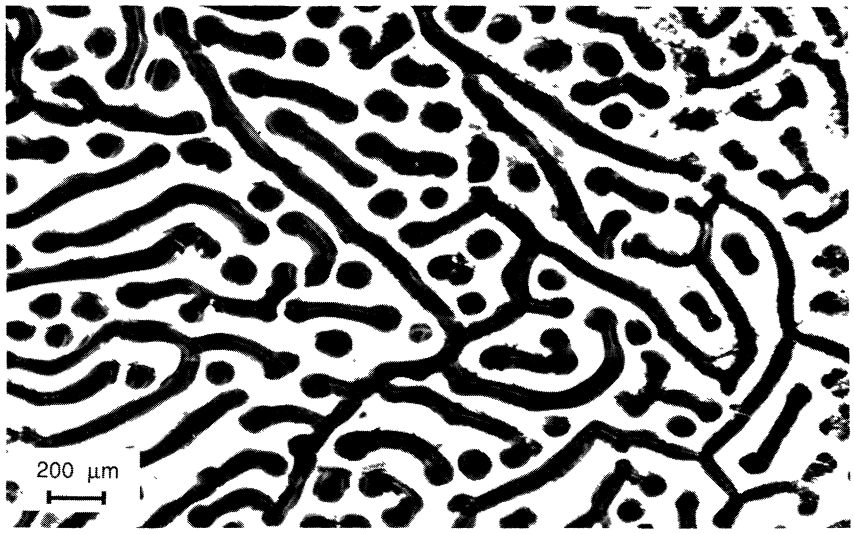

Fig. 5. — Elongated cells $V = 0.65$ cm/h.

Elongated cells are observed for $V = 0.65$ cm/h (Fig. 5). These cells do not form an array but rather a labyrinth of wavy channels, similar to what is commonly observed in other instabilities, e.g. in ferrofluids [24]. From observations on a number of binary alloys (see e.g. Refs. [25, 26]), it is known that such a structure indicates that we are just above the onset of morphological instability, which we thus estimate at $V_C = 0.60 \pm 0.05$ cm/h. As the segregation coefficient is close to unity, this limit is weakly shifted towards lower V by convection. From the Mullins-Sekerka criterion $GDK/mV_C C_\infty(K-1) = S$ [21], where $G_L \approx 2 K_L G_L/(K_L + K_S)$ and the stability function $S = 0.7$ from figure 2, a value $K \approx 1.2$ can be deduced which is only 8 % higher than what can be *estimated* from Hansen's diagram [27]. Nevertheless, this difference results in a $\Delta(K-1)/(K-1) \approx 1$ so that the magnitude of the destabilizing influence of solutal convection on the threshold cannot be estimated as it is buried in the uncertainty on $K - 1$.

A direct measurement on the elongated cells gives a width of 140 µm which is about forty

per cent of the critical wavelength λ_{MS} for $K = 1.1$, which is given by the Mullins-Sekerka theory, and $V_C = 0.6$ cm/h

$$\lambda_{MS} = \left(\frac{2\,\Gamma D^2}{mC_\infty (K-1)} \right)^{1/3} 2\,\pi V_C^{-2/3}. \tag{7}$$

This value is an upper estimate since the critical velocity is higher under diffusion control. As the bifurcation is supercritical for Pb-30 % Tl alloys, this discrepancy can be attributed to the effect of convection which is known to decrease the periodicity [28, 29].

The elongated cells exist only over a narrow interval and give way to hexagonal cells at $V \approx 1.15\,V_C$. Imperfect hexagonal arrays of cells are observed for velocities ranging from 0.75 to 1.1 cm/h (Fig. 6a). The structures grow parallel to the direction of pulling, whatever the crystallographic orientation of the solid. The cellular to dentritic transition occurs at

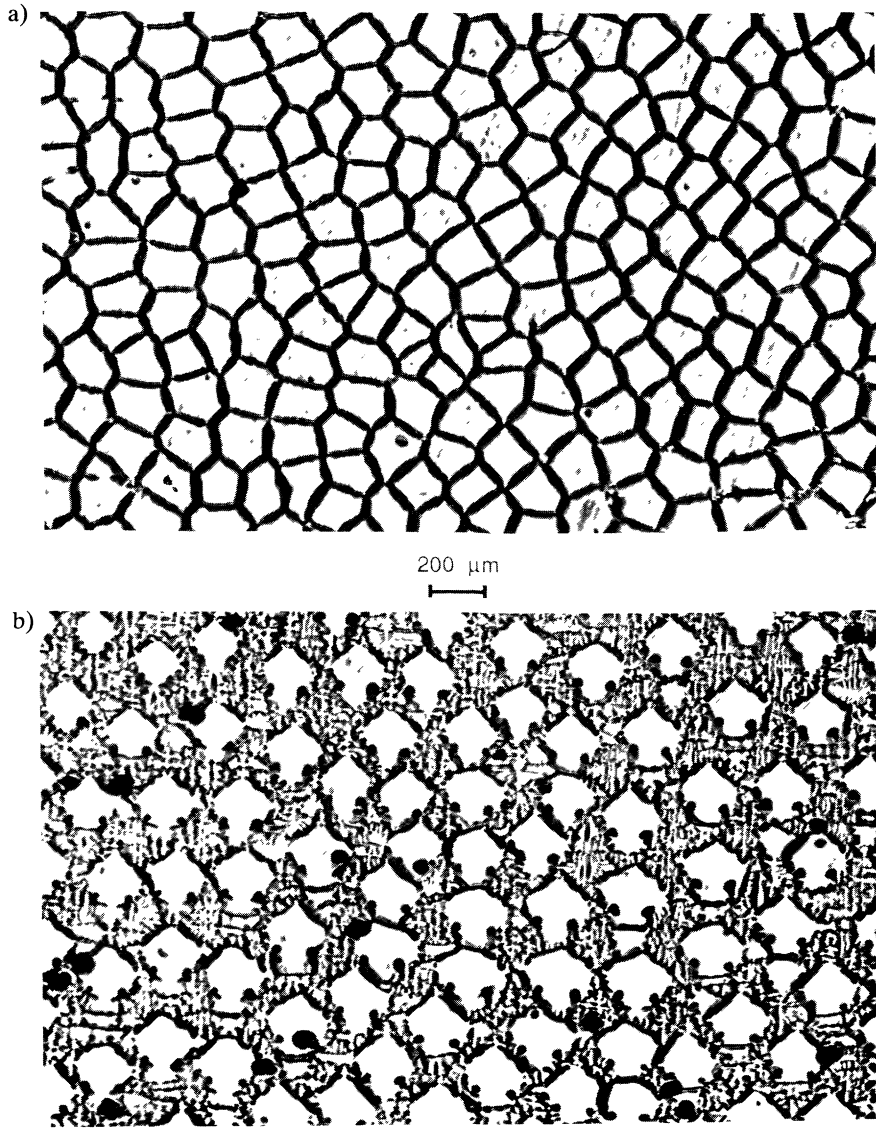

Fig. 6. — a) Cells $V = 1.10$ cm/h. b) Dendrites $V = 2.00$ cm/h.

$V = 2\,V_C$. Dendrites grow in a [100] direction, at an angle with the vertical. When the [100] direction is close enough to the vertical, the Wigner-Seitz method can still be used to reconstruct the dendritic array and determine the periodicity λ (Fig. 6b).

3. Array characteristics.

3.1 PRIMARY SPACING. — Despite solutal convection in the melt, only a negligible variation of the primary spacing is observed on a transverse section. Nevertheless, for a safe comparison between the different samples, the periodicity λ is always measured in the central part of the section, where the macroscopic modulation of the front is weak and nearly axisymmetric [19]. As far as the primary spacing is concerned, cells and dendrites belong to the same regime for the range of velocities considered in this study (Fig. 7). A least-square fitting through these data points gives a variation which is almost linear

$$\lambda \div V^{0.94}. \tag{8}$$

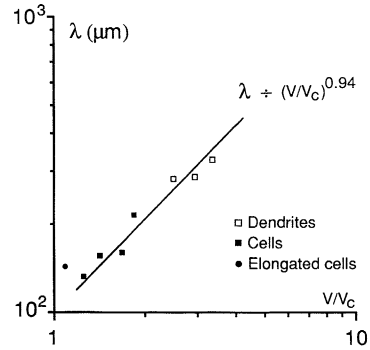

Fig. 7. — Variation of the primary spacing λ with V/V_C.

Equation (8) is similar to what is obtained by a least-square fitting through the data points of Miyata *et al.* on Al-Cu alloys [30] which, like the present Pb-Tl alloys, were grown with convection in the fluid phase. Besides, it results from a comparative study of dendritic growth of Al-Cu alloys grown at 1 g and under microgravity that the primary spacing decreases with V under diffusive transport in the melt whereas λ shows an opposite behaviour when the transport is mainly convective [18]. We thus consider that it is likely that, besides the reduction of the periodicity, convection rules out the regime and thus imposes the scaling law for λ for both cells and dendrites.

These results should be compared to experiments carried out under pure diffusive transport in the melt, e.g. to succinonitrile-acetone alloys grown in Hele-Shaw cells for which [4]

$$\lambda \div V^{-0.34} \tag{9}$$

for the dendritic regime, for which no significant difference in behaviour has to our knowledge been ever evidenced between 2D and 3D samples solidified in the absence of convection (see e.g. Refs. [31, 32]). Moreover, the dendritic transition occurs at the maximum value of λ so that cells and dendrites then belong to different regimes.

Let us notice that this comparison cannot be extended to any shape parameter. Indeed, the diffusive law for the tip radius R seems to be valid in the whole dendritic range for Al-Cu

alloys (see Fig. 4 of Ref. [30]), even in the region where convection scales the primary spacing. This suggests that there might be different behaviours with respect to convection for the aray and the tip regions whose lengthscales are λ and R respectively.

There is a paucity of theoretical analyses of the influence of the fluid flow on periodicity. The boundary-layer analysis of Rouzaud and Favier of the morphological stability of the solidification interface under convective conditions [33] cannot be used because we have no diffusive boundary layer and are too far from the threshold. Dupouy *et al.* have derived a relation for the case of convection in a porous dendritic array [28]

$$\lambda \div V^{0.5} . \tag{10}$$

This law is not verified by the present experiments probably because the array is not actually porous, with deep and large interdendritic liquid channels. Indeed, the width of the two-phase region is about 100 μm which is of the order of the primary spacing λ.

3.2 MICROSTRUCTURAL ORDER.

3.2.1 *Defects.* — The nature and number of defects which are present in a cellular or dendritic array are easily obtained from the Wigner-Seitz reconstruction (Fig. 4). Polygons having from 4 to 8 sides are identified. All but those with 6 sides are considered as defects. Pentagons and heptagons are far more numerous and the most common defect is the pentagon-heptagon pair which, when isolated, is analog to an edge dislocation in a honeycomb, to which a Burgers vector **b** can be associated (Fig. 8). Actually, grain boundaries are seen which consist of a succession of pentagon-heptagon pairs.

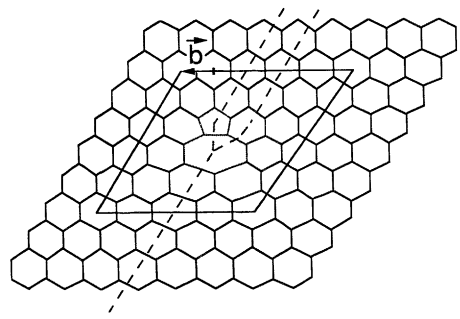

Fig. 8. — Basic pentagon-heptagon pair forming a dislocation in the array. The Burger's circuit and associated vector **b** are indicated.

For cellular growth, the percentages of the different types of polygons (Tab. II) correspond to the average values over five Wigner-Seitz reconstructions, one for the very central part of the transverse section and four in the adjacent annulus, at ninety degrees from one another. Therefore, the standard deviation associated with each value is representative of the global uncertainty due to the manual plotting of the cell centers and to the inhomogeneity of the 3D-array on the macroscopic scale, which is essentially linked to convection. From the figures in table II, it follows that both uncertainties are small enough for a pertinent discussion of the trends for hexagons and pentagons and heptagons. For dendrites, two protruding solid areas are observed which are associated with the two principal convective rolls [19]. Consequently,

Table II. — *Defect analysis.*

V cm/s	V/V_C	d_S %	squares %	pentagons %	hexagons %	heptagons %	octagons %
0.75	1.25	55	3 ± 1	27 ± 4	45 ± 5	22 ± 2	3 ± 1
0.85	1.42	53	2 ± 1	24 ± 3	47 ± 4	25 ± 2	2 ± 1
1.00	1.67	51	3 ± 1	23 ± 3	49 ± 3	22 ± 3	3 ± 1
1.10	1.83	51	1 ± 1	26 ± 4	49 ± 4	22 ± 3	2 ± 2
1.50	2.50	49	2	25	51	18	4
1.75	2.92	45	2	21	55	19	3
2.00	3.33	49	1	22	51	23	3

the values are taken from the reconstruction of only the solid area of larger extent, which appears first and is more homogeneous.

The main result is that the percentage d_S of defects is very important and apparently depends neither on convection, (since it does not depend on Rayleigh number which varies significantly with V), nor on the level v. Such high d_S are a first indication of the « liquid » character of the patterns. Indeed, the response of the patterns to a typical method of analysis of the configurations obtained from 2D-melting simulations is qualitatively similar to that of a 2D-liquid. The regular honeycomb which would exist for a « 2D-solid » array is actually « melted » by the defects, from which the aspect of the translational and orientational correction functions will follow, as it will be seen in the next section.

For Bénard-Marangoni convection a different behaviour is observed [22]. Indeed, the patterns are well organized near the onset and disorder progressively increases with distance to the instability threshold. Nevertheless, it should be noticed that d_S is very sensitive to the experimental procedure which is used to establish the structures and that great care has to be taken in order to achieve a low d_S just above the threshold [34]. Our results are for *standard* experiments of directional solidification so that it is still an open question whether an optimized procedure, which would lead to lower d_S, is feasible or not.

In other words, it would be worth to know the time dependence of d_S. If there is some analogy with Bénard-Marangoni convection, d_S is likely to slowly decrease with time by the transient elimination of defects by pair annihilation and on the periphery, down to a limit value characteristic of v. Yet, such a process would be very difficult to follow on a massive metallic sample of *limited length*. Moreover, the more blurred the cellular walls in the directionally solidified part, the farther one proceeds from the quench.

3.2.2 *Correlation functions.* — The order of the array is characterized by translational and orientational correlation functions [23, 35]

$$G(\mathbf{r}) = \langle \rho_G(\mathbf{r})\, \rho_G(0) \rangle \tag{11a}$$

and

$$G_6(\mathbf{r}) = \langle \Psi_6(\mathbf{r}) \cdot \Psi_6(0) \rangle / |\Psi_6(0)|^2 \tag{11b}$$

which are defined over all the cells. These functions respectively involve a translational order parameter

$$\rho_{\mathbf{G}}(\mathbf{r}) = \exp[i\mathbf{G} \cdot \mathbf{u}(\mathbf{r})] \tag{12a}$$

and an order parameter for bond orientation [23]

$$\Psi_6(\mathbf{r}) = \frac{1}{6} \sum_{j=1}^{6} \exp[6\, \theta_j\, \mathbf{r}]\,. \tag{12b}$$

$\rho_{\mathbf{G}}(\mathbf{r})$ is the local Fourier component of cell-center density at a reciprocal lattice vector $\mathbf{G}$ and $\mathbf{u}$ is the displacement of a cell from its regular position $\mathbf{r}$. The factor 6 in equation (12b) stems from the hexagonal symmetry of the lattice and θ is an angle relative to an arbitrary axis.

Typical correlation functions are shown in figure 9 for the beginning and end of the cellular range, which reflect the absence of translational order and orientational order for both cases. For short-range order of the patterns, as for a 2D-liquid, the envelopes of $G(\mathbf{r}) - 1$ decay to zero as $\exp(-r/\zeta)$ where ζ is the correlation length. The orientational correlation function $G_6(\mathbf{r})$ can be fitted by an exponential law $G_6(\mathbf{r}) \div \exp(-\alpha r)$, whereas it would be constant for a cellular array with long-range order, i.e. alike a 2D-solid.

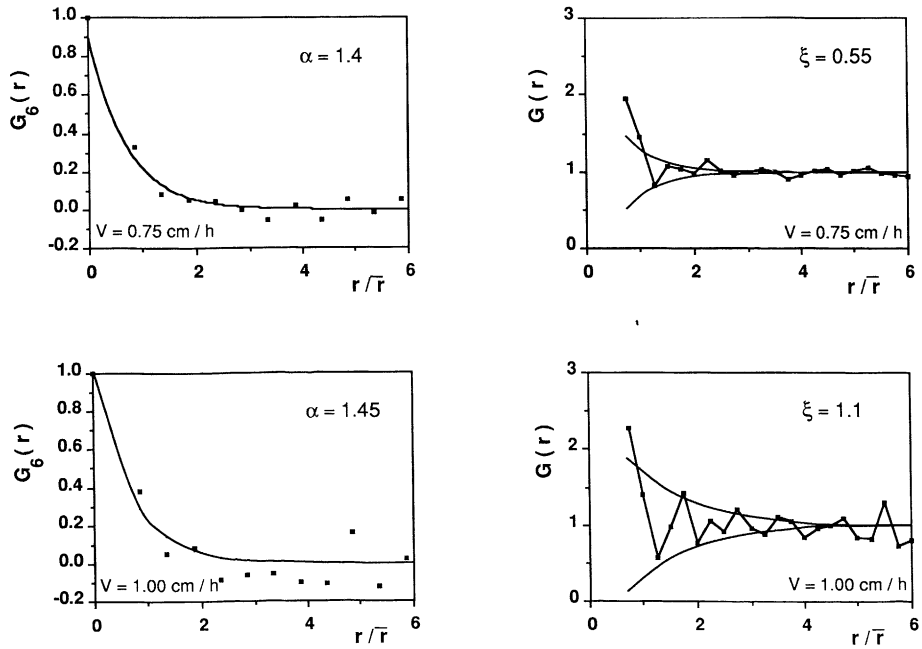

Fig. 9. — Orientational correlation function $G_6(\mathbf{r})$ and translational correlation function $G(\mathbf{r})$.

In order to estimate the error bars in the determination of ζ and α, which result from the imprecision in the evaluation of $G_6(\mathbf{r})$ and $G(\mathbf{r})$, several fits have been done by changing the number of points involved in the computation. The resulting values for ζ and α respectively are $\zeta = 0.55 \pm 0.20$, $\alpha = 1.4 \pm 0.1$ for $V = 0.75$ cm/h and $\zeta = 1.1 \pm 0.1$, $\alpha = 1.45 \pm 0.15$ for $V = 1$ cm/h. These values are of the same order of magnitude as those determined by Occelli

et al. for a Bénard-Marangoni array with $d_S = 25$ %, $\zeta = 0.56$ and $\alpha = 0.4$ [23]. Once again, the short correlation lengths ζ and high damping factors α, which are presently obtained for cells, simply reflect the strong disorder of the honeycombs formed in directional solidification.

4. Conclusion.

Characteristics of cellular and dendritic arrays are determined on lead-30 wt% thallium alloys grown with solutal-driven convection in the liquid phase. For the first time in directional solidification, a Wigner-Seitz reconstruction is performed which, besides an accurate determination of the primary spacing, enables the analysis of the defects and of the order of the arrays. The major results are :

(i) a regime is evidenced in which the variation of the periodicity λ with the growth velocity is dominated by convection. Cells and dendrites then obey the same relationship, which is opposed to what is observed for solidification under diffusive transport in the melt ;

(ii) the basic defects are polygons with less, or more, than six sides. Pentagon-heptagon pairs usually form chains which are equivalent to grain boundaries. The percentage of defects is high so that the array can be considered as « melted » ;

(iii) the translational and orientational correlation functions are typical of only a short-range order.

The present observations illustrate the gap between current theoretical approaches, which consider a *unique* spacing, and the real experimental situation. The last two points indicate that the cellular arrays are far from being perfect honeycombs, which might be a clue to the understanding of pattern selection. Indeed, it cannot be excluded that the defects play a role in the dynamics of the adjustement of the *average* primary spacing to a steady-state value.

Acknowledgements.

Stimulating discussions with P. Cerisier and R. Occelli are gratefully acknowledged. Special thanks are due to R. Occelli who initiated us to the practical use of the Wigner-Seitz reconstruction and of the correlation functions.

The authors are indebted to the Centre National d'Etudes Spatiales for the financial support of this work.

References

[1] LANGER J. S., Chance and Matter, Les Houches Summer School. Proceedings, Eds. J. Souletie and J. Vannimenus (Elsevier, Amsterdam) vol. **46** (1988).
[2] KESSLER D. A., KOPLIK J. and LEVINE H., *Adv. Phys.* **37** (1988) 255.
[3] PELCÉ P., Dynamics of Curved Fronts (Academic Press, Boston) 1988.
[4] BILLIA B. and TRIVEDI R., *J. Cryst. Growth,* submitted.
[5] TRIVEDI R., *J. Cryst. Growth* **49** (1980) 219.
[6] BILLIA B., JAMGOTCHIAN H. and CAPELLA L., *J. Cryst. Growth,* submitted.
[7] MULLINS W. W. and SEKERKA R. F., *J. Appl. Phys.* **35** (1964) 444.
[8] TILLER W. A., JACKSON K. A., RUTTER J. W. and CHALMERS B., *Acta Met.* **1** (1953) 428.
[9] DE CHEVEIGNÉ S., GUTHMANN C. and LEBRUN M. M., *J. Cryst. Growth* **73** (1985) 242.
[10] WOLLKIND D. J. and SEGEL L. A., *Phil. Trans. Roy. Soc. London* **268** (1970) 251.
[11] CAROLI B., CAROLI C. and ROULET B., *J. Phys.* **43** (1982) 1767.
[12] UNGAR L. H. and BROWN R. A., *Phys. Rev. B* 29 (1984) 1367 ; **31** (1985) 5931.
[13] CORIELL S. R., CORDES M. R., BOETTINGER W. J. and SEKERKA R. F., *J. Cryst. Growth* **49** (1980) 13.

[14] HURLE D. T. J., JAKEMAN E. and WHEELER A. A., *J. Cryst. Growth* **58** (1982) 163.
[15] CAROLI B., CAROLI C., MISBAH C. and ROULET B., *J. Phys. France* **46** (1985) 401.
[16] HENNENBERG M., ROUZAUD A., FAVIER J. J. and CAMEL D., *J. Phys. France* **48** (1987) 173.
[17] MCFADDEN G. B., CORIELL S. R. and BOISVERT R. F., *Phys. Fluids* **28** (1985) 2716.
[18] GUÉRIN R. Z., BILLIA B., HALDENWANG P. and ROUX B., *Phys. Fluids* **31** (1988) 2086.
[19] NGUYEN THI H., BILLIA B. and JAMGOTCHIAN H., *J. Fluid Mech.* **204** (1989) 581.
[20] JAMGOTCHIAN H., BILLIA B. and CAPELLA L., *J. Cryst. Growth* **62** (1983) 539.
[21] SEKERKA R. F., *J. Appl. Phys.* **36** (1965) 264.
[22] JAMGOTCHIAN H., BILLIA B. and CAPELLA L., *J. Cryst. Growth* **82** (1987) 342.
[23] OCCELLI R., GUAZZELLI E. and PANTALONI J., *J. Phys. Lett. France* **44** (1983) 567.
[24] BACRI J. C., PERZYNSKI R. and SALIN D., *La Recherche* **192** (1987) 1150.
[25] MORRIS L. R. and WINEGARD W. C., *J. Cryst. Growth* **5** (1969) 361.
[26] BILONI H., Physical Metallurgy, Ed. R. W. Cahn and P. Haasen (North-Holland, Amsterdam) 1983, Ch. 9.
[27] HANSEN M., Constitution of Binary Alloys (McGraw-Hill, New York) 1958, p. 1115.
[28] DUPOUY M. D., CAMEL D. and FAVIER J. J., *Acta Met.* **37** (1989) 1143.
[29] MCCAY M. H., LEE J. E. and CURRERI P. A., *Met. Trans. A* **17** (1986) 2301.
[30] MIYATA Y., SUZUKI T. and UNO J. I., *Met. Trans. A* **16** (1985) 1799.
[31] SOMBOONSUK T., MASON J. T. and TRIVEDI R., *Metall. Trans. A* **15** (1984) 967.
[32] MASON J. T., VERHOEVEN J. D. and TRIVEDI R., *Metall. Trans. A* **15** (1984) 1665.
[33] FAVIER J. J. and ROUZAUD A., *J. Cryst. Growth* **64** (1983) 367.
[34] OCCELLI R., private communication.
[35] KOSTERLITZ J. M. and THOULESS D. J., *J. Phys. Colloq. france* **34** (1973) C6-1181.